Featured Article

Delineation of Brain Tumor Extent with [^{11}C]L-Methionine Positron Emission Tomography: Local Comparison with Stereotactic Histopathology

Lutz W. Kracht,[1] Hrvoje Miletic,[2] Susanne Busch,[1] Andreas H. Jacobs,[3] Jurgen Voges,[4] Moritz Hoevels,[4] Johannes C. Klein,[1] Karl Herholz,[3] and Wolf-D. Heiss[1,3]

[1]Max-Planck-Institute for Neurological Research, Cologne; and Department of [2]Neuropathology, [3]Neurology, and [4]Stereotactic Neurosurgery, University of Cologne, Cologne, Germany

ABSTRACT

Purpose: **Methyl-[^{11}C]L-methionine ([^{11}C]MET) positron emission tomography (PET) in brain tumors reflects amino acid transport and has been shown to be more sensitive than magnetic resonance imaging in stereotactic biopsy planning. It remains unclear whether the increased [^{11}C]MET uptake is limited to solid tumor tissue or even detects infiltrating tumor parts.**

Experimental Design: **In 30 patients, a primary or recurrent brain tumor was suspected on magnetic resonance imaging. Patients were investigated with [^{11}C]MET-PET before stereotactic biopsy. The biopsy trajectories were plotted into the [^{11}C]MET-PET images with a newly designed C-based software program. The exact local [^{11}C]MET uptake was determined within rectangular regions of interest of 4 mm in width and length aligned with the biopsy specimen. Individual histologic specimens were rated for the presence of solid tumor tissue, infiltration area, and nontumorous tissue changes.**

Results: **Receiver operating characteristics analysis demonstrated a sensitivity of 87% and specificity of 89% for the detection of tumor tissue at a threshold of 1.3-fold [^{11}C]MET uptake relative to normal brain tissue. At this threshold, only 13 of 100 tumor positive specimen were false negative mainly in grade 2 astrocytoma. In grade 2 astrocytoma, mean [^{11}C]MET uptake in the infiltration area was significantly higher than in solid tumor tissue ($P < 0.003$).**

Conclusions: **[^{11}C]MET-PET detects solid parts of brain tumors, as well as the infiltration area at high sensitivity and specificity. High [^{11}C]MET uptake in infiltrating tumor of astrocytoma WHO grade 2 reflects high activity in this tumor compartment. Molecular imaging, with [^{11}C]MET, will guide improved management of patients with brain tumors.**

INTRODUCTION

In the treatment of brain tumors, the balance between tumor destruction and preservation of brain function is particularly delicate because of their invasive growth and the lack of curative treatment for most of them. Thus, therapeutic intervention is primarily palliative and, therefore, must preserve or improve brain function, rather than sacrificing it for tumor treatment of limited efficacy. On the other hand, tumor treatment should be as aggressive and effective as possible to gain survival time, with the extent of surgical resection still being one of the most important prognostic factors (1). Assessing this delicate balance requires detailed information on tumor location and extent. In general, contrast-enhanced magnetic resonance imaging (MRI) or computed tomography (CT) serve to define the tumor margins. Contrast enhancement reflects regions of breakdown of blood-brain barrier and is taken as a surrogate marker for active tumor tissue. Still, contrast enhancement is an inaccurate indicator of active tumor. It is falsely negative in viable tumor parts that do not show blood-brain barrier breakdown, and it is falsely positive in necrotic or inflamed areas with blood-brain barrier disruption. Serial biopsies of patients undergoing craniotomy for malignant gliomas have shown tumor cells at a distance of >3 cm away from CT contrast enhancement (2, 3). Moreover, MRI spectroscopy data also suggest that standard T1-weighted contrast-enhanced MRI may underestimate the volume of metabolically active tumors (4). T2-weighted MRI abnormalities, previously believed to represent edema only, are known to include microscopic disease extension, as verified by biopsy studies by Kelly *et al.* (3). In conclusion, advanced therapeutic strategies such as neuronavigation in neurosurgery, brachytherapy with stereotactically implanted isotopes, or conventional radiotherapy need a more accurate definition of tumor extent for target volume planning than provided by standard MRI or CT.

Many studies have shown that the margins of tumors, as assessed by positron emission tomography (PET) with amino acid tracers such as methyl-[^{11}C]L-methionine ([^{11}C]MET), are frequently wider than those assessed by MRI or CT (5). This phenomenon is even more pronounced in low-grade tumors and in diffuse gliomatosis because of their frequent lack of contrast enhancement in MRI (6). Also, in comparison with [^{18}F]-2-fluoro-2-deoxy-D-glucose, better tumor delineation is reported for amino acid tracers (7).

Received 2/10/04; revised 7/2/04; accepted 8/4/04.
The costs of publication of this article were defrayed in part by the payment of page charges. This article must therefore be hereby marked *advertisement* in accordance with 18 U.S.C. Section 1734 solely to indicate this fact.

Requests for reprints: Wolf-D. Heiss, Max-Planck-Institute for Neurologic Research, Gleueler Str. 50, D-50931 Cologne, Germany. Phone: 49-221-4726-220; Fax: 49-221-4726-349; E-mail: wdh@pet.mpin-koeln.mpg.de.

[^{11}C]MET is incorporated into most brain tumors, even into low-grade gliomas, and is being used in the management of patients with gliomas (8, 9). [^{11}C]MET is a sensitive tracer in tumor detection, and it differentiates benign from malignant lesions with high sensitivity and specificity with relatively low background activity in normal brain tissue (5, 10). [^{11}C]MET uptake correlates to cell proliferation in cell culture (11), Ki-67 expression (12), proliferating cell nuclear antigen expression (13), and microvessel density (14), indicating its role as a marker for active tumor proliferation and angiogenesis.

Increased amino acid uptake in gliomas is not a direct measure of protein synthesis but rather seems to be due to increased transport mediated by type L amino acid carriers. Miyagawa *et al.* (15) demonstrated in a rat tumor model that facilitated transport of amino acids is up-regulated and suggested that tumors can influence transporter expression in their vasculature.

Stereotactic biopsies guided by [^{11}C]MET-PET are more successful in finding tumor tissue than CT-only guided ones (16). Mosskin *et al.* (17) in 1987 could demonstrate that [^{11}C]MET-PET accurately delineated the tumor in 22 of 31 cases when compared with histologic findings in stereotactic biopsies, but scanner resolution with 8-mm full width at half maximum and a slice thickness of 11 mm was low at that time.

In high-grade gliomas, areas with anaplastic changes have higher [^{11}C]MET uptake than tumor samples without histologic signs of anaplasia (18). Presence of necrosis in the anaplastic samples may cause a decreased [^{11}C]MET uptake (18). Yet, it is still unclear whether the area of increased tracer uptake is restricted to solid tumor tissue or extends into infiltrating tumor parts when compared with normal brain or nontumorous tissue.

Localization of the exact position of a stereotactic biopsy sample in PET imaging data are difficult. In previous studies, procedures, including PET, CT, surgical planning, and biopsy, all needed to take place on the same day with a stereotactic head ring fixed (18) Mosskin *et al*. (17) used an individually molded plastic helmet that snaps into the PET and CT scanners to perform PET investigation and surgical procedure on consecutive days. In both instances, practicability and patient discomfort limited its applicability.

We developed a procedure for accurate projection of biopsy trajectories into MRI and [^{11}C]MET-PET imaging data after stereotactic biopsy. This allowed an exact local comparison of the extent of signal changes in structural and functional imaging data and histopathological findings in the biopsy specimen without any additional strain for the patients.

PATIENTS AND METHODS

Patients. In this retrospective study thirty patients (age, 40 $\pm$ 8.9 years; 16 female, 14 male) were investigated with [^{11}C]MET-PET within 2 years. Because PET studies were part of the preoperative diagnostic procedure, approval by the Institutional Review Board was not required. Twenty-two patients suffered from a newly diagnosed brain tumor, and in 8 patients, recurrent glioma was suspected after MRI. Six of the patients with recurrent disease had undergone radiation therapy.

One of the eight patients diagnosed with glioblastoma WHO grade 4 had progressed to secondary glioblastoma from a former grade 2 astrocytoma. The other seven patients were diagnosed with newly developed or recurrent primary *de novo* glioblastoma (19). In a patient with grade 2 ependymoma and suspected recurrence, biopsy demonstrated normal brain tissue and in two patients no tumor could be confirmed in biopsy specimen.

After stereotactic biopsy, all patients received a final histologic diagnosis according the WHO grading system (20). Individual patient data are given in Table 1, and histologic diagnoses are summarized in Table 2.

Imaging. All patients underwent [^{11}C]MET-PET and MRI before stereotactic biopsy. The median time between [^{11}C]MET-PET and stereotactic biopsy was 9 days (range, 1 to 35 days). PET studies were performed either on an ECAT EXACT HR or ECAT EXACT scanner (Siemens-CTI, Knoxville, TN; refs. 21, 22) as previously described by Herholz *et al.* (8). After a 10-minute transmission scan, 740 MBq (20 mCi) [^{11}C]MET, synthesized according to the method of Berger *et al.* (23), were injected i.v. Tracer accumulation was recorded in thee-dimensional mode over 60 minutes in 47 transaxial slices from the entire brain. Summed activity from 20 to 60 minutes after tracer injection was used for image reconstruction. Images were reconstructed with fourier rebinning and filtered back projection with a ramp filter. Images were corrected for scatter, attenuation, and random coincidences. Spatial resolution was 6 mm or better in all dimensions. MRI was performed on a 1.5-T system (Gyroscan ACS-NT or Gyroscan Intera; Philips Medical Systems, Best, the Netherlands) with the standard quadrature head coil. A typical magnetic resonance examination consisted of axial T2-weighted turbo spin-echo and T1-weighted spin-echo post contrast images with a slice thickness of 2 mm and a matrix size of 512 $\times$ 512 pixels (voxel size, 0.5 $\times$ 0.5 $\times$ 2.0 mm).

In all patients, [^{11}C]MET-PET was performed as part of imaging procedures for presurgical biopsy planning. The preoperative MRI was linked with images of an intraoperative stereotactic CT (24). One to three computer-assisted (STP 3.5; Stryker-Leibinger, Freiburg, Germany) trajectories for stereotactic biopsy were defined (25–27). In 13 patients, [^{11}C]MET-PET data were integrated directly into the trajectory planning procedure, and trajectories were defined on [^{11}C]MET-PET. The location of biopsy was documented on stereotactic X-ray images and a hardcopy of the computer assisted planning procedure.

Image Processing. For exact local comparison of signal changes in presurgical PET and MRI, the biopsy trajectories were visualized in the preoperative planning MRI. A C-based program was developed using the following data: (*a*) preoperative digital MRI images; (*b*) landmark-based transformation parameters of preoperative MRI to the stereotactic coordinate system as defined during surgery planning; and (*c*) the target and entry point of biopsies. The preoperative MRI was transformed by a landmark based algorithm to the stereotactic coordinate system provided by intraoperative CT (24). Then, the target and entry points of the trajectories used for biopsies were calculated within native coordinates of the original MRI data set. Voxels in the biopsy needle trajectory connecting both points were set to a fixed intensity with a width of two voxels

Table 1 Individual patient data

Patient ID	Age (y)	Histological diagnosis	WHO grade	Localization	No. of specimens	Newly diagnosed (ND)/ recurrence (REC)	Rx *	Time between [^{11}C]MET PET and surgery (days)
pat01	56	Astrocytoma	2	Right thalamus	4	ND	No	31
pat02	44	Astrocytoma	2	Right frontal	5	REC	No	30
pat03	23	Astrocytoma	2	Left frontal	5	ND	No	34
pat04	36	Astrocytoma	2	Right frontal	12	REC	Yes	1
pat05	57	Astrocytoma	2	Left fronto-temporal, thalamus	5	ND	No	5
pat06	29	Astrocytoma	3	Left frontal	3	ND	No	1
pat07	31	Astrocytoma	3	Right fronto-parietal	2	REC	No	14
pat08	63	Astrocytoma	3	Left temporo- parietal	3	ND	No	31
pat09	32	Astrocytoma	3	Right fronto-parietal	4	ND	No	2
pat10	23	Astrocytoma	3	Right fronto-parietal	5	ND	No	8
pat11	30	Astrocytoma	3	Left fronto-parietal	5	ND	No	10
pat12	69	Astrocytoma	3	Left frontal	3	ND	No	35
pat13	67	Glioblastoma	4	Left parietal	6	REC	Yes	3
pat14	65	Glioblastoma	4	Right temporal	2	ND	No	7
pat15	64	Glioblastoma	4	Left fronto-parietal	4	ND	No	15
pat16	58	Glioblastoma	4	Left frontal	7	REC	Yes	29
pat17	46	Glioblastoma	4	Right temporal	4	ND	No	11
pat18	37	Glioblastoma	4	Left fronto-parietal, thalamus	3	ND	No	1
pat19	57	Glioblastoma	4	Left frontal	4	ND	No	9
pat20	58	Glioblastoma	4	Right occipital	3	REC	Yes	4
pat21	52	Oligodendroglioma	2	Left frontal	5	ND	No	5
pat22	56	Oligodendroglioma	3	Left frontal	4	ND	No	8
pat23	13	Ependymoma	2	Right cerebellum	2	REC	Yes	35
pat24	19	Ganglioglioma	1	Left occipital	7	REC	No	2
pat25	67	CNS lymphoma		Left temporal	4	ND	No	2
pat26	60	CNS lymphoma		Left frontal, temporal	4	ND	No	21
pat27	53	CNS lymphoma		Left cerebellum	3	ND	No	5
pat28	51	Melanoma		Right fronto-parietal	4	ND	No	2
pat29	50	Demyelination		Left fronto-parietal	4	ND	No	14
pat30	45	Demyelination		Right occipital	3	ND	No	18

NOTE. Individual data of 30 patients with suspected newly diagnosed or recurrent brain tumor who underwent serial stereotactic biopsy after [^{11}C]MET-PET. Number of specimens includes those that were not suitable for examination.

* Radiation therapy before [^{11}C]MET-PET.

Abbreviation: CNS, central nervous system.

(Fig. 1*A*). Correct positioning of the trajectories was checked against the hardcopies of the planning procedure.

[^{11}C]MET images were coregistered with the computed trajectory magnetic resonance images with an interactive program (Multi Purpose Imaging Tool; ref. 28). PET image and trajectory magnetic resonance images were rotated to show the complete biopsy trajectory on either the axial, coronar, or sagittal view (Fig. 1, *A* and *B*). The position and length of each biopsy specimen documented during surgery was determined along the individual trajectories. For each specimen, local [^{11}C]MET uptake was determined within a rectangular region of interest of 4 mm in width and the length of the biopsy specimen (Fig. 1*C*). Length of biopsies ranged between 4 and 7 mm. Additionally, a circular region of interest of 7 mm in diameter was placed in the area of maximum [^{11}C]MET uptake. Within each region of interest, mean uptake was determined relative to a corresponding contralateral control region. Every specimen was rated for the presence or absence of contrast enhancement in enhanced T1-weighted MRI.

Histopathology. Tumor specimens were classified according to the WHO classification scheme for brain tumors (20). Distinct histologic criteria were established for characterization of biopsy specimens and correlation with PET data: the biopsies were assessed for presence of solid tumor and brain tissue with infiltrating tumor cells. A solid tumor was characterized for the presence of gemistocytic tumor cells. Brain tissue with infiltrating tumor cells was additionally classified by distinguishing white and/or gray matter. The vascularization of the biopsy specimen was classified separately and subdivided into normal and tumor vascularization. Tumor vascularization was addition-

Table 2 Histological diagnoses

Histological diagnosis and WHO grade	No. of patients	No. of biopsy specimens
Astrocytoma 2	5	26
Astrocytoma 2	7	24
Glioblastoma 4	8	29
Oligodendroglioma 2	1	5
Oligodendroglioma 3	1	4
Primary central nervous system lymphoma	3	10
Ganglioglioma 1	1	7
Ependymoma 2	1	2
Metastasis	1	4
Demyelination	2	7
Total	30	118

NOTE. Number of patients and number of suitable biopsies within tumors of different histological type and WHO grade and nontumorous lesions.

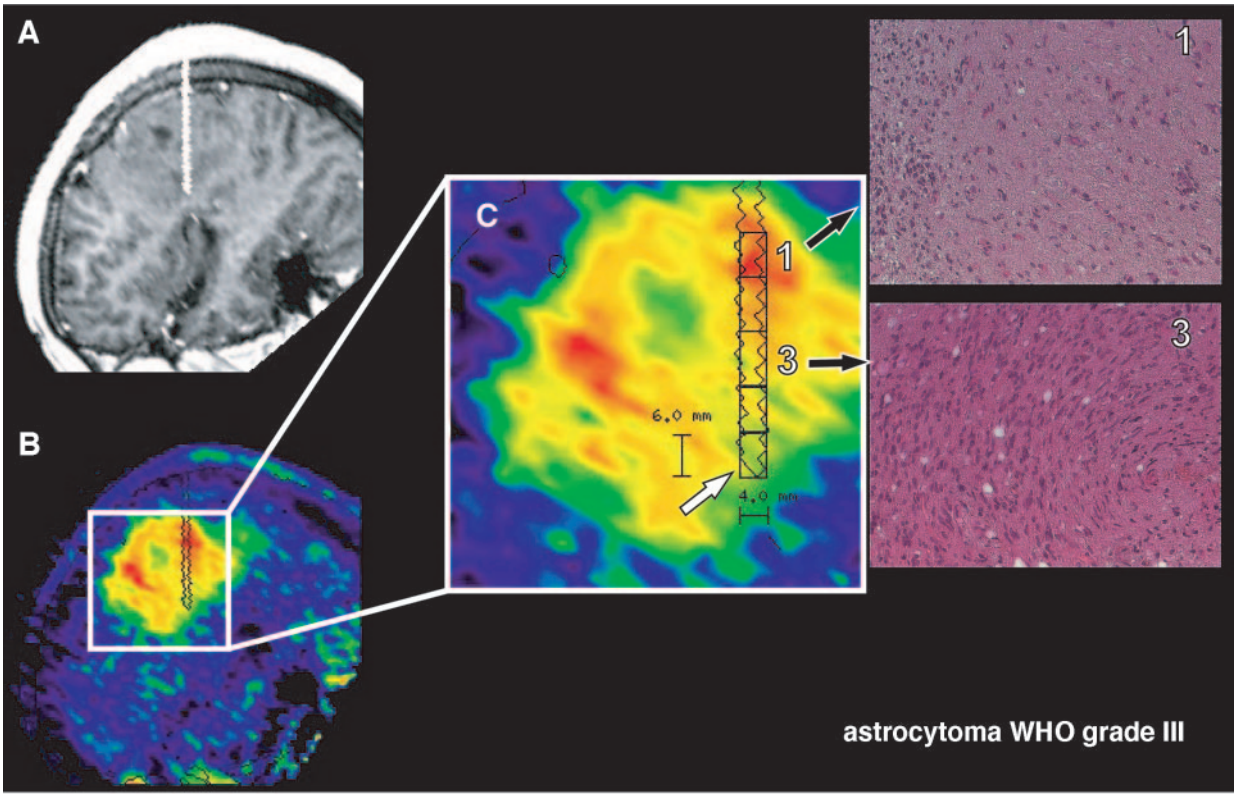

Fig. 1 Illustration of image processing. Biopsy trajectory is projected into the preoperative MRI image (*A*). The [^{11}C]MET-PET image is resliced to fit to the magnetic resonance image, and the biopsy trajectory is visualized and projected into the fused PET/magnetic resonance image (*B*). Magnification of [^{11}C]MET-PET (*C*) demonstrates how regions of interest were defined. A rectangular region of interest with 4 mm in width and the individual length of each specimen (*C*, in this example, 6 mm, *white arrow*) are placed at the exact position of each biopsy specimen, and the mean [^{11}C]MET uptake was calculated. This patient was newly diagnosed with astrocytoma grade 3 showing no contrast enhancement on MRI (*A*). [^{11}C]MET uptake was higher in the area of tumor infiltration (biopsy 1) compared with solid tumor (biopsy 3).

ally differentiated in beginning proliferation, clear proliferation, and glomeruloid-like proliferation of the endothelium. Furthermore, branching of capillaries in oligodendroglial tumors was described. Nontumorous histopathological findings were classified as normal brain tissue or reactive brain tissue with gliosis, demyelination, necrosis, or inflammation.

For statistical analyses SPSS, version 10.0.7 (SPSS, Inc., Chicago, IL) was used, and graphs were plotted with SigmaPlot, version 7.0 (SPSS, Inc.).

RESULTS

Tumor Delineation. A total of 129 biopsy specimens was investigated. Eleven specimens were not suitable for histopathological examination. To determine the relative [^{11}C]MET uptake value that best distinguishes tumor (including solid tumor and brain tissue with infiltrating tumor cells, 100 specimens) from nontumorous brain tissue (18 specimens), receiver operating characteristic analysis was performed by varying the threshold of [^{11}C]MET uptake over the whole range of values and calculating sensitivity and specificity for each value (Fig. 2).

The best cutoff was found at a threshold of 1.3 relative [^{11}C]MET uptake with a sensitivity of 87% [95% confidence

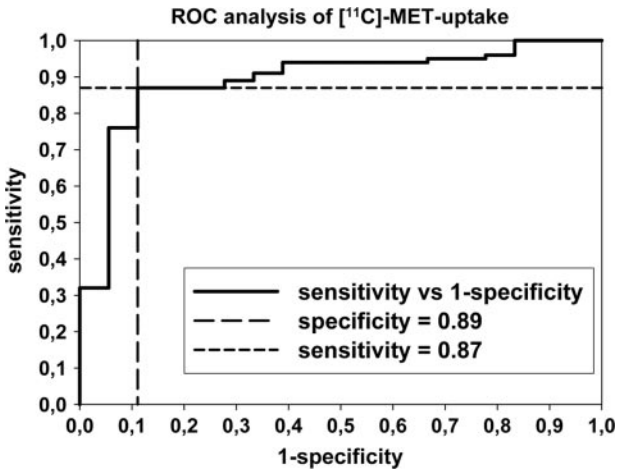

Fig. 2 Receiver operating characteristic (ROC) analysis of exact local [^{11}C]MET uptake for the differentiation of tumor tissue from nontumorous biopsy areas. [^{11}C]MET uptake was varied over the whole range of values, and sensitivity and specificity were calculated for each value. At a threshold of 1.3, the sensitivity was 0.87 and the specificity was 0.89, respectively.

interval (CI), 80–93] and a specificity of 89% (95% CI, 72.2–100; area under the curve, 0.89; 95% CI, 0.81–0.97). At this threshold, only 13 of 100 tumor-positive specimens were classified false negative mainly in low-grade astrocytomas (23% of specimens). Fifty-seven of 66 (86%, 95% CI, 77.2–93.9) specimen from solid tumor and 30 of 34 (88%, 95% CI, 76.5–97.1) from infiltrating tumor specimen were classified correct positive. In 20 patients with astrocytic gliomas, 8 of 10 false negative specimens were located in solid tumor tissue with five specimens from astrocytoma WHO grade 2. In malignant astrocytoma WHO grade 3 and glioblastoma WHO grade 4, only 3 of 29 specimens from solid tumor were false negative.

One specimen demonstrating necrosis next to a solid glioblastoma was classified false positive with a relative [^{11}C]MET uptake of 1.48. In a patient with primary central nervous system lymphoma, high [^{11}C]MET uptake (2.13) was detected in an area with normal cerebellar cortex next to infiltrating tumor tissue. The only false positive finding in a patient with nontumorous disease showed demyelination in histology, but the area of highest uptake (relative [^{11}C]MET 1.50) was not represented in the stereotactic biopsy. In 10 patients, the area of highest [^{11}C]MET uptake was not included in the biopsy specimen. In one patient, the biopsy specimen mainly demonstrated lymphocytic inflammation with a small proportion of polymorphic cells with atypical nuclei. In a fraction of these cells, p53–protein was detected by immunohistochemistry. The tumor was finally diagnosed as an anaplastic astrocytoma WHO grade 3, but additional differentiation between solid tumor and infiltration was impossible. Two patients with suspected recurrent glioblastoma after surgery and radiation therapy demonstrated a high relative [^{11}C]MET uptake of 2.31 and 3.31. Specimens were diagnosed as gliosis with infiltration of a glial tumor and were counted positive because of this tumor infiltration. The typical pattern of a glioblastoma with vascular proliferation and necrosis was not present. At follow-up, both patients showed continuous tumor progression on MRI and [^{11}C]MET-PET. Biopsy in one patient 3 months later showed the typical pattern of a glioblastoma.

Table 3 Maximum relative [^{11}C]MET uptake within different tumors

Histological diagnosis and WHO grade	No. of patients	Maximum [^{11}C]MET uptake (mean ± SD)
Astrocytoma 2	5	1.80 ± 0.35
Astrocytoma 3	7	2.39 ± 0.55
Glioblastoma 4	8	2.41 ± 0.48
Oligodendroglioma 2	1	2.07
Oligodendroglioma 3	1	2.10
Ganglioglioma 1	1	1.65
Central nervous system lymphoma	3	3.35–4.11
Melanoma metastases	1	3.14
Nontumor lesions*	3	1.05–1.50

NOTE. Maximum [^{11}C]MET uptake within tumors of different histological type and WHO grade and nontumorous lesions. The maximum was defined in the area of highest [^{11}C]MET uptake independent of biopsy localization, and the ratio to the corresponding contralateral region was calculated.

* Two patients with demyelation and one patient with suspected recurrent ependymoma WHO grade 2 but normal brain tissue and minor reactive changes in biopsy specimen.

Table 4 Relative [^{11}C]MET uptake within individual compartments of gliomas

Histological diagnosis and WHO grade	Infiltration (*N*) (mean ± SD)	Solid tumor (*N*) (mean ± SD)
Astrocytoma 2 *	1.72 ± 0.22 (9)	1.30 ± 0.35 (12)
Astrocytoma 3	2.48 ± 0.69 (4)	1.90 ± 0.61 (15)
Glioblastoma 4	1.74 ± 0.52 (13)	1.96 ± 0.47 (14)
Nontumor tissue	1.09 ± 0.36 (18)	

NOTE. Mean [^{11}C]MET uptake within different tumor subcompartments of gliomas of different WHO grade and nontumorous tissue. [^{11}C]MET uptake was defined in the exact local position of each biopsy specimen, and the ratio to the corresponding contralateral region was calculated.

* Difference of [^{11}C]MET uptake between infiltration and solid tumor statistically significant in Student's *t* test, $P = 0.003$.

Abbreviation: *N*, number of biopsies.

[^{11}C]MET-Uptake in Tumor Compartments. The maximum relative [^{11}C]MET uptake in the different histologic entities of tumors was comparable with previous findings and is shown in Table 3 (8). [^{11}C]MET uptake in subcompartments of the tumors is summarized in Table 4. In grade 2 astrocytoma, mean [^{11}C]MET uptake in the infiltration area was significantly higher (Student's *t* test, $P = 0.003$) than in solid tumor tissue. In grade 3 anaplastic astrocytoma, uptake in the area of infiltration differed from uptake in solid tumor (2.48 ± 0.69 *versus* 1.90 ± 0.61), but the difference did not reach statistical significance (Student's *t* test, $P = 0.129$; Fig. 1). No such statistical significant difference was observed in patients with glioblastoma (Table 4). Highest maximum [^{11}C]MET uptake was seen in three patients with primary central nervous system lymphoma ranging from 3.35 to 4.11. Nine of 10 specimens were clearly delineated with a mean relative [^{11}C]MET uptake of 2.98 ± 0.70 overall 9 tumor specimens. One metastasis of a malignant melanoma presented with high [^{11}C]MET uptake in all four specimens from solid tumor ranging from 2.78 to 2.93.

Signs of vascular proliferation were present in grade 3 gliomas and grade 4 glioblastomas. In these tumors, there was no significant difference of [^{11}C]MET uptake between areas with vascular proliferation and tissue specimens without typical signs of endothelial proliferation. Specimens without endothelial proliferation often demonstrated an increased number of vessels.

Gemistocytic cell populations were detected in two patients suffering from astrocytomas only. One of them demonstrated a relative [^{11}C]MET uptake of 2.30, which is relatively high compared with other astrocytomas of WHO grade 2. Additionally, this patient had contrast enhancement on MRI in the area of one specimen, whereas no contrast enhancement was observed in the other 25 specimens of grade 2 astrocytomas.

In grade 3 anaplastic astrocytomas and grade 4 glioblastomas, 29 of 53 biopsy specimens were taken from areas with no signs of contrast enhancement. Twenty-five of these 29 specimens originated from solid tumor parts. There was no significant difference of relative [^{11}C]MET uptake between contrast enhancing tissue (1.89 ± 0.60) and non–contrast-enhancing tissue (1.88 ± 0.56) in this sample.

DISCUSSION

The results of receiver operating characteristic analysis indicate that [^{11}C]MET-PET detects solid parts of brain tumors, as well as the infiltration area with high sensitivity (87%) and specificity (89%). This proves the superior properties of [^{11}C]MET-PET in delineating the tumor extent in a direct local comparison with histopathological changes. Thus, [^{11}C]MET-PET is an excellent tool for treatment planning in neurosurgery, stereotaxy, or radiation therapy to guide the delicate balance between effective tumor elimination and preservation of brain function. In addition, the information derived from [^{11}C]MET-PET about the extent of active tumor tissue may be useful in monitoring systemic chemotherapy.

Current therapeutic strategies in the treatment of brain tumors, such as stereotactic radiation therapy, stereotactic brachytherapy, and neuronavigation in general neurosurgery, use preoperative imaging data, mainly from MRI and CT, to identify the target tumor tissue. The delineation properties of MRI or CT for the definition of tumor extent are poor. Usually, the contrast enhancement on standard contrast-enhanced T1-weighted MRI or CT, reflecting the breakdown of the blood-brain barrier, is used as a surrogate marker for active tumor tissue. However, there are concerns about the validity of this assumption, especially because active tumor tissue can be found in regions where such a breakdown of the blood-brain barrier has not occurred (2–4). Because [^{11}C]MET uptake by normal brain parenchyma is low, [^{11}C]MET-PET is superior to [^{18}F]-2-fluoro-2-deoxy-D-glucose-PET in the assessment of tumor dimensions (17, 18, 29). Bergstrom *et al.* (29) described a patient with an anaplastic astrocytoma who was examined with CT and PET with [^{68}Ga]EDTA, [^{11}C]glucose, and [^{11}C]MET. The patient died 15 days after the [^{11}C]MET-PET, and histologic evaluation at autopsy showed excellent agreement between tumor extent and [^{11}C]MET uptake. More than 50% of the tumor would not have been detected without the [^{11}C]MET-PET (29). Studies integrating [^{11}C]MET-PET images in radiation therapy planning procedures confirm these discrepancies between MRI, CT, and [^{11}C]MET-PET (30, 31).

Herholz *et al.* (8) described a threshold of 1.47 with a sensitivity of 76% and specificity 87% for the discrimination of brain tumors from nontumoral brain lesions. In the present study with exact local comparison of histopathological changes and [^{11}C]MET uptake within brain lesions, the threshold for differentiation of tumor tissue from nontumor tissue is somewhat lower with an increased sensitivity and specificity when compared with the in the previous study (8). Patients that are referred to stereotactic biopsy are preselected and only patients where a nontumorous lesion such as inflammation, hemorrhage, or ischemic stroke cannot be excluded by other diagnostic procedures undergo stereotactic biopsy. This might explain the different thresholds for discrimination of brain tumors from nontumoral brain lesions (8) and for differentiation of tumor tissue from nontumor tissue within brain lesions in our study.

Because of ethical reasons no biopsies can be taken from areas that are not suspect of containing tumor, thus limiting the number of tumor-free biopsies. At a threshold of 1.3 in our study sensitivity was 87% with a 95% CI from 80 to 93, and specificity was 89% (95% CI, 72.2–100). This means that there is a remaining uncertainty with regard to correct classification in the order of 20 to 25% that should be kept in mind.

In grade 2 astrocytoma relative [^{11}C]MET uptake at a threshold of 1.30 underestimated tumor extent in ~25% of tissue samples. Low [^{11}C]MET uptake in a proportion of grade 2 astrocytomas is a known feature of this histologic entity (8).

Diameter of biopsies is only 1-2 mm and is not clearly represented even in high-resolution positron cameras such as the ECAT EXACT HR with a transaxial resolution of 3.6-mm full width at half maximum at the center of the field of view. Thus, tumor tissue with only slightly increased [^{11}C]MET uptake might be hidden by normal brain uptake, and nontumor tissue next to highly accumulating tumor parts might show false positive [^{11}C]MET uptake. Previous studies used PET cameras with 8-mm full width at half maximum and a slice thickness up to 11 mm. Modern scanners provide 3.6-mm full width at half maximum and a slice thickness of 3.125 mm (ECAT EXACT HR), resulting in improved delineation properties of [^{11}C]MET uptake compared with the already good properties reported by Mosskin *et al.* (17). One false positive finding was observed in a necrotic area. It was located next to solid tumor tissue with high [^{11}C]MET uptake. Therefore, its high uptake might be because of partial volume effect. Another patient with acute demyelination was falsely classified positive by [^{11}C]MET-PET. A small number of acute inflammatory lesions with mild [^{11}C]MET uptake have been observed in previous studies (8, 32).

With regards to differences of [^{11}C]MET uptake in the tumor subcompartments, astrocytomas WHO grade 2 demonstrated significantly higher [^{11}C]MET uptake in infiltration area compared with solid tumor tissue. Low-grade astrocytomas are slowly growing tumors with only a mildly increased cell count and low proliferative activity. Areas where astrocytoma cells penetrate brain parenchyma show a dynamic interplay of processes such as cell-cell adhesion, proteolytic remodeling, synthesis of extracellular matrix, and expression and activation of growth factors and integrins (33, 34). Increased [^{11}C]MET uptake in areas of tumor invasion might reflect a higher demand for amino acids such as methionine for these processes compared with the slowly growing solid tumor tissue of low-grade astrocytomas. This is underlined by the fact that tumors with high microvessel density and the ability to recruit and modulate vasculature show increased [^{11}C]MET uptake (14).

High microvessel density does not necessarily correlate with signs of endothelial proliferation (35). In this study, vascular proliferation was per definition restricted to anaplastic astrocytoma grade 3 and glioblastoma grade 4, and there was no difference of [^{11}C]MET uptake between tissue with and without endothelial proliferation, but specimens without signs of endothelial proliferation often demonstrated stronger vascularization.

Endothelial proliferation and necrosis are associated with breakdown of the blood-brain barrier and often show contrast enhancement in MRI or CT (3, 29). Twenty-nine of 53 specimens in malignant astrocytoma grade 3 and 4 presented with no signs of contrast enhancement but showed increased [^{11}C]MET uptake similar to findings of Bergstrom *et al.* (29) who demonstrated that >50% of the tumor would have not been detected on contrast enhanced CT alone. MRI and CT are necessary for stereotactic biopsy planing because morphologic information of

location of blood vessels and eloquent brain areas is needed, and therefore, [^{11}C]MET-PET is an additional investigation that can give important information about target for biopsy and tumor extent to the neurosurgeon but cannot be evaluated without MRI.

In two patients with preirradiated recurrent glioblastoma, only gliosis with infiltrating tumor cells was represented in tissue specimens in contrast to high [^{11}C]MET uptake. At follow-up, both patients had continuous tumor progression according to MRI and [^{11}C]MET-PET, and biopsy from one patient 3 months later showed the typical pattern of a glioblastoma. Biopsy specimens might not have been representative of the actual tumor mass in these patients. On the other hand, high [^{11}C]MET uptake could reflect remaining tumor activity after radiation before formation of new solid tumor tissue.

Histologic classification of samples has been proved challenging in a number of cases where it was difficult to differentiate between reactive gliosis and tumor infiltration mainly consisting of gliosis with sparsely scattered tumor cells. Vascularity was often increased without signs of endothelial proliferation.

One patient with gemistocytic variant of grade 2 astrocytoma had the highest [^{11}C]MET uptake of all low-grade astrocytomas that might reflect the more aggressive behavior of this tumor type with its tendency to earlier malignant progression compared with other histologic subtypes (36).

In conclusion, [^{11}C]MET-PET detects solid parts of brain tumors, as well as areas of infiltration with high sensitivity and specificity. Limited diagnostic accuracy only occurs in patients astrocytomas WHO grade 2 only. In this histologic subtype, [^{11}C]MET uptake is significantly higher in the infiltrating tumor parts compared with solid tumor tissue, most likely reflecting relatively high tumor activity in this area. Molecular imaging with [^{11}C]MET-PET will improve diagnoses and management of patients with gliomas and is an excellent method to perform image guided therapy.

REFERENCES

1. Nazzaro JM, Neuwelt EA. The role of surgery in the management of supratentorial intermediate and high-grade astrocytomas in adults. J Neurosurg 1990;73:331–44.

2. Burger PC, Heinz ER, Shibata T, et al. Topographic anatomy and CT correlations in the untreated glioblastoma multiforme. J Neurosurg 1988;68:698–704.

3. Kelly PJ, Daumas-Duport C, Scheithauer BW, et al. Stereotactic histologic correlations of computed tomography- and magnetic resonance imaging-defined abnormalities in patients with glial neoplasms. Mayo Clin Proc 1987;62:450–9.

4. Pirzkall A, McKnight TR, Graves EE, et al. MR-spectroscopy guided target delineation for high-grade gliomas. Int J Radiat Oncol Biol Phys 2001;50:915–28.

5. Jacobs AH, Winkler A, Dittmar C, et al. Molecular and functional imaging technology for the development of efficient treatment strategies for gliomas. Technol Cancer Res Treat 2002;1:187–204.

6. Mineura K, Sasajima T, Kowada M, et al. Innovative approach in the diagnosis of gliomatosis cerebri using carbon-11-L-methionine positron emission tomography. J Nucl Med 1991;32:726–8.

7. Kaschten B, Stevenaert A, Sadzot B, et al. Preoperative evaluation of 54 gliomas by PET with fluorine-18-fluorodeoxyglucose and/or carbon-11-methionine. J Nucl Med 1998;39:778–85.

8. Herholz K, Holzer T, Bauer B, et al. 11C-methionine PET for differential diagnosis of low-grade gliomas. Neurology 1998;50:1316–22.

9. Weber WA, Wester HJ, Grosu AL, et al. *O*-(2-[18F]fluoroethyl)-L-tyrosine and L-[methyl-11C]methionine uptake in brain tumours: initial results of a comparative study. Eur J Nucl Med 2000;27:542–9.

10. Jager PL, Vaalburg W, Pruim J, et al. Radiolabeled amino acids: basic aspects and clinical applications in oncology. J Nucl Med 2001; 42:432–45.

11. Langen KJ, Muhlensiepen H, Holschbach M, et al. Transport mechanisms of 3-[123I]iodo-alpha-methyl-L-tyrosine in a human glioma cell line: comparison with [3H]methyl]-L-methionine. J Nucl Med 2000;41: 1250–5.

12. Chung JK, Kim YK, Kim SK, et al. Usefulness of 11C-methionine PET in the evaluation of brain lesions that are hypo- or isometabolic on 18F-FDG PET. Eur J Nucl Med Mol Imaging 2002;29:176–82.

13. Sato N, Suzuki M, Kuwata N, et al. Evaluation of the malignancy of glioma using 11C-methionine positron emission tomography and proliferating cell nuclear antigen staining. Neurosurg Rev 1999;22: 210–4.

14. Kracht LW, Friese M, Herholz K, et al. Methyl-[11C]-L-methionine uptake as measured by positron emission tomography correlates to microvessel density in patients with glioma. Eur J Nucl Med Mol Imaging 2003;30:868–73.

15. Miyagawa T, Oku T, Uehara H, et al. "Facilitated" amino acid transport is up-regulated in brain tumors. J Cereb Blood Flow Metab 1998;18:500–9.

16. Pirotte B, Goldman S, David P, et al. Stereotactic brain biopsy guided by positron emission tomography (PET) with [F-18]fluorodeoxyglucose and [C-11]methionine. Acta Neurochir Suppl (Wien) 1997; 68:133–8.

17. Mosskin M, von Holst H, Bergstrom M, et al. Positron emission tomography with 11C-methionine and computed tomography of intracranial tumours compared with histopathologic examination of multiple biopsies. Acta Radiol 1987;28:673–81.

18. Goldman S, Levivier M, Pirotte B, et al. Regional methionine and glucose uptake in high-grade gliomas: a comparative study on PET-guided stereotactic biopsy. J Nucl Med 1997;38:1459–62.

19. Kleihues P, Ohgaki H. Primary and secondary glioblastomas: from concept to clinical diagnosis. Neuro-oncol 1999;1:44–51.

20. Kleihues P, Cavenee WK. Pathology and genetics of tumours of the nervous system (WHO). Lyon, France: International Agency for Research on Cancer (IARC Press); 2000.

21. Wienhard K, Eriksson L, Grootoonk S, et al. Performance evaluation of the positron scanner ECAT EXACT. J Comput Assist Tomogr 1992;16:804–13.

22. Wienhard K, Dahlbom M, Eriksson L, et al. The ECAT EXACT HR: performance of a new high resolution positron scanner. J Comput Assist Tomogr 1994;18:110–8.

23. Berger G, Maziere M, Knipper R, et al. Automated synthesis of 11C-labelled radiopharmaceuticals: imipramine, chlorpromazine, nicotine and methionine. Int J Appl Radiat Isot 1979;30:393–9.

24. Ende G, Treuer H, Boesecke R. Optimization and evaluation of landmark-based image correlation. Phys Med Biol 1992;37:261–71.

25. Backlund EO. A new instrument for stereotaxic brain tumour biopsy. Technical note. Acta Chir Scand 1971;137:825–7.

26. Schlegel W, Scharfenberg H, Sturm V, et al. Direct visualization of intracranial tumours in stereotactic and angiographic films by computer calculation of longitudinal CT-sections: a new method for stereotactic localization of tumour outlines. Acta Neurochir (Wien) 1981;58:27–35.

27. Voges J, Schroder R, Treuer H, et al. CT-guided and computer assisted stereotactic biopsy. Technique, results, indications. Acta Neurochir (Wien) 1993;125:142–9.

28. Pietrzyk U, Herholz K, Schuster A, et al. Clinical applications of registration and fusion of multimodality brain images from PET, SPECT, CT, and MRI. Eur J Radiol 1996;21:174–82.

29. Bergstrom M, Collins VP, Ehrin E, et al. Discrepancies in brain tumor extent as shown by computed tomography and positron emission tomography using [68Ga]EDTA, [11C]glucose, and [11C]methionine. J Comput Assist Tomogr 1983;7:1062–6.

30. Grosu AL, Lachner R, Wiedenmann N, et al. Validation of a method for automatic image fusion (BrainLAB System) of CT data and 11C-methionine-PET data for stereotactic radiotherapy using a LINAC: first clinical experience. Int J Radiat Oncol Biol Phys 2003;56:1450–63.

31. Nuutinen J, Sonninen P, Lehikoinen P et al. Radiotherapy treatment planning and long-term follow-up with [(11)C]methionine PET in patients with low-grade astrocytoma. Int J Radiat Oncol Biol Phys 2000; 48:43–52.

32. Dethy S, Manto M, Kentos A, et al. PET findings in a brain abscess associated with a silent atrial septal defect. Clin Neurol Neurosurg 1995;97:349–53.

33. Rao JS. Molecular mechanisms of glioma invasiveness: the role of proteases. Nat Rev Cancer 2003;3:489–501.

34. Tysnes BB, Mahesparan R. Biological mechanisms of glioma invasion and potential therapeutic targets. J Neurooncol 2001;53:129–47.

35. Folkerth RD. Descriptive analysis and quantification of angiogenesis in human brain tumors. J Neurooncol 2000;50:165–72.

36. Schiffer D, Chio A, Giordana MT, et al. Prognostic value of histologic factors in adult cerebral astrocytoma. Cancer (Phila.) 1988; 61:1386–93.